IR Optical Properties of Pt Nanoparticles and Their Agglomerates Investigated by in Situ FTIRS Using CO as the Probe Molecule

Wei Chen, Shi-Gang Sun,* Zhi-You Zhou, and Sheng-Pei Chen

State Key Lab for Physical Chemistry of Solid Surfaces, Department of Chemistry, Xiamen University, Xiamen 361005, China

Received: March 23, 2003; In Final Form: July 5, 2003

Pt nanoparticles (Pt_n) and their agglomerates (Pt_n^{ag}) were synthesized by chemical reduction methods. The mean sizes of Pt_n and Pt_n^{ag} were determined to be respectively 3.4 and 400 nm using transmission electron microscopy (TEM). CO adsorption on electrodes made of the two kinds Pt nanomaterials was used as the probe reaction. Studies of cyclic voltammetry revealed that the current peak potential of CO_{ad} oxidation on electrodes of Pt_n^{ag} supported on glassy carbon (Pt_n^{ag}/GC) has been shifted negatively by about 80 mV in comparison with that on a bulk Pt electrode. In situ electrochemical FTIRS results illustrated that Pt_n/GC and Pt_n^{ag}/GC exhibit different IR properties for CO adsorption. In comparison with CO adsorbed on bulk Pt, a phenomenon of enhanced IR absorption (EIRA) was observed on dispersed Pt nanoparticles (Pt_n). IR absorption of CO_{ad} on Pt_n/GC is enhanced 31 times and the full width at half-maximum (FWHM) of the CO_L band is increased to 40 cm^{-1}, which is 25 cm^{-1} larger than the value (15 cm^{-1}) measured on a bulk Pt electrode. In contrast to the EIRA of CO adsorbed on dispersed Pt nanoparticles, the abnormal infrared effects (AIREs) were encountered for CO adsorbed on agglomerates of Pt nanoparticles, in which a strong interaction is presented between Pt_n. The IR features of CO adsorbed on Pt_n^{ag}/GC illustrated that, except for the IR absorption of CO_{ad} being enhanced 9 times and the FWHM of the CO_L band being increased to 25 cm^{-1}, the direction of the CO_{ad} bands is inverted from absorption to antiabsorption. The results of the present paper demonstrated that the EIRA and the AIREs are closely related to the agglomerate states of Pt nanoparticles, and throw a light on the origin of the particular IR properties of nanomaterials.

Introduction

There has been a long-standing interest in metal nanoparticles, because their characteristic properties are significantly different not only from those of the corresponding bulk metals but also from those of atoms. Such nanomaterials possess many potential applications in optical, electronic, and magnetic devices as well as catalysts, photocatalysts, and sensors.[1−5] Up to the present stage, substantial progresses in studies concerning metal nanoparticles have been achieved, e.g., the synthesis of stable and monodispersed nanoparticle suspension, the characterization of microstructure and the investigation of diverse properties. The preparation, characterization and the application of metal nanoparticles in catalysis and electrocatalysis have received extensive attention in recent years.[6−8] From an experimental point of view, it is difficult to prepare metal nanoparticles in the perfect monodispersed state. Among most studies focused on the efforts to make monodispersed nanoparticles,[9−15] in fact some show that aggregates of nanoparticles, for example, those of Au and Ag, display different optical properties from those of dispersed nanoparticles. In a study carried out by Storhoff and co-workers,[16] the gold nanoparticle aggregates have been characterized by a reduced extinction in the UV, violet, and blue region and by a red shifted and broadened plasmon peak with respect to that of the dispersed nanoparticle. Similar studies also have been published further by other groups.[17−20] Owing to the unique catalytic properties, platinum group metals were frequently used in fuel cells as an anode for electrooxidation of hydrogen or other small organic molecules and also as a cathode for electroreduction of oxygen.[21] The electrocatalysts in fuel cells and other applications often use platinum or platinum alloy nanoparticles dispersed on a conductive substrate in the form of a thin film. In a series of publications, Sun et al.[22−28] have reported that nanometer scale thin film materials of platinum group metals (Pt, Pd, and Rh) and their alloys (PtPd, PtRu) exhibit abnormal IR properties that are named abnormal infrared effects (AIREs). The AIREs have been discovered in the studies of chemisorption of CO or other species (e.g., SCN^-, POPD etc.) on nanometer scale thin film electrodes and manifest primarily by three abnormal IR features when compared to CO or other molecules adsorbed on corresponding bulk metals; the three features are the antiabsorption (the inversion of the direction of CO_{ad} bands), the enhancement of IR absorption, and the increase in discreteness of vibration energy states (the increase in IR bandwidth). AIREs have been observed also for CO adsorbed on a nanostructured Rh film at solid−gas interfaces.[29] A related phenomenon is the so-called surface-enhanced IR absorption (SEIRA)[30] discovered initially in the IR study of *p*-nitrobenzoic acid adsorbed on a Ag film of island structures formed on a Si substrate; IR absorption of some vibration modes are significantly enhanced. The SEIRA has been confirmed mainly on films of coinage metals with island structures (mainly Au and Ag),[31,32] and recently in the case of CO adsorbed on Pd nanoparticles confined in the supercage of Y-zeolite.[33] The major difference in IR features between the AIREs and the SEIRA is that the direction of adsorbate IR bands in the AIREs is inverted; i.e., the direction of IR bands is

* Corresponding author. Fax: +86 592 2183047. E-mail: sgsun@xmu.edu.cn.

10.1021/jp034740g CCC: $25.00
Published on Web 08/19/2003

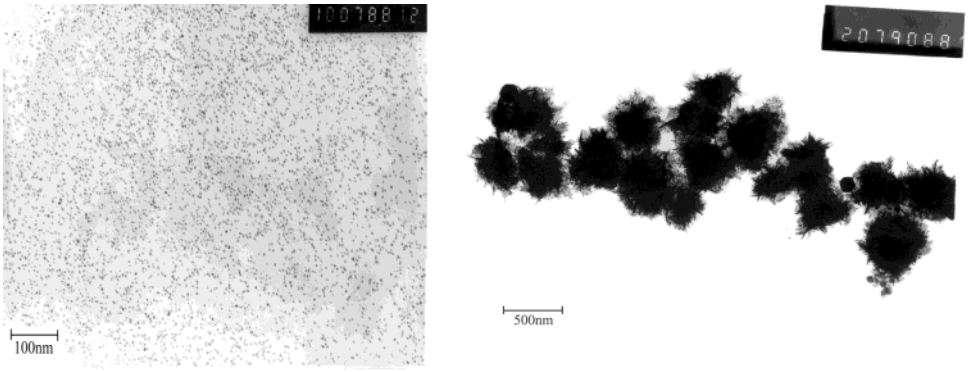

Figure 1. TEM patterns of Pt nanoparticles (a) and the agglomerates of Pt nanoparticles (b).

changed from the direction of absorption to that of emission (or antiabsorption). It is evident that the difference in IR features between the AIREs and the SIREA are related to different chemical compositions and structures of thin films. To clarify further the origin of the AIREs, we have prepared electrodes consisting of thin films made of Pt nanoparticles or agglomerates of Pt nanoparticles; using CO adsorption as the molecular probe, the investigation was conducted with electrochemical cyclic voltammetry and in situ FTIR reflection spectroscopy. In this paper we wish to report that dispersed Pt nanoparticles produce enhanced IR absorption, whereas agglomerates of Pt nanoparticles exhibit abnormal infrared effects for CO chemisorption.

Experimental Section

Preparation of Electrodes. The Pt nanoparticles (denoted as Pt_n) used in these experiments were prepared by reducing hexachloroplatinic acid hexahydrate ($H_2Pt_2Cl_6 \cdot 6H_2O$) with methanol to metallic Pt and were stabilized with poly(vinylpyrrolidone) (PVP). The agglomerates of Pt nanoparticles (denoted as Pt_n^{ag}) were synthesized by reducing $H_2Pt_2Cl_6 \cdot 6H_2O$ to Pt with H_2 gas bubbling into the solution that contained Nafion as stabilizer. Nafion also acted as an agent to fix Pt_n^{ag} on a substrate surface to form a thin film.

Glassy carbon (GC) was polished mechanically using sandpaper and alumina powders of size 5 and 1 down to 0.3 μm before the deposition of Pt_n and Pt_n^{ag} onto its surface. A prescribed quantity of suspension of Pt_n was applied to the surface of such a GC substrate, upon which a drop of 0.5% (V/V) Nafion solution was dispersed to fix Pt_n on the surface. Separately, a prescribed quantity of suspension of Pt_n^{ag} was applied to the surface of the GC substrate; the Pt_n^{ag} was automatically fixed as indicated above. In both cases, a thin film was formed on the GC substrate after solvent evaporation. The electrodes thus prepared were denoted as Pt_n/GC and Pt_n^{ag}/GC, respectively.

Electrochemical in Situ Fourier Transform Infrared Reflection Spectroscopy (in Situ FTIRS). In situ FTIR spectroscopic measurements were carried out on a Nexus 870 FTIR spectrometer (Nicolet) equipped with an EverGlo IR source and a liquid nitrogen-cooled MCT-A detector. A CaF_2 disk was used as the IR window, and a thin layer of solution was formed by moving the electrode toward the IR window during FTIR measurements. The incident angle of the infrared beam was aligned at about 60°. In all measurements the potential difference technique was employed. The multistep FTIRS (MS-FTIR) procedure was used in the present study.[34] In this procedure a series of single-beam spectra were collected first at sample potentials (E_S), where adsorbed CO is stable, and a single-beam spectrum was collected finally at reference potential (E_R), at which adsorbed CO has been removed completely by electrooxidation. The resulting spectra were calculated using

$$\frac{\Delta R}{R} = \frac{R(E_S) - R(E_R)}{R(E_R)} \quad (1)$$

$R(E_S)$ and $R(E_R)$ are single-beam spectra of reflection collected at sample potential E_S and reference potential E_R, respectively. Each single-beam spectrum was recorded by collecting and co-adding 400 interferograms at a spectral resolution of 8 cm^{-1}, which will take ca. 2.8 min with the moving mirror velocity of 3.16 cm s^{-1}.

Other Experimental Conditions. Transmission electron microscopy (TEM) patterns were obtained with a JEM-100CX-II electron microscopy operating at an acceleration voltage of 100 kV. The cyclic voltammetric studies were carried out with an XHD-II potentiostat (Department of Chemistry, Xiamen University), at a potential scan rate of 50 mV s^{-1}. Solutions (0.1 M H_2SO_4) were prepared from Millipore water and super pure H_2SO_4. Before each measurement the solution was deaerated by bubbling pure N_2 for 20 min. Then the solution was saturated with high-purity CO (99.95%) by continuously purging. The reference electrode used was a saturated calomel electrode (SCE), and potentials reported in the present paper were those with respect to the SCE scale. All experiments were carried out at room temperature.

Results and Discussion

1. TEM Characterization of Pt Nanoparticles and Their Agglomerates. Figure 1 shows typical transmission electron micrographs of Pt_n and Pt_n^{ag}. Ligands or polymers, especially solvent-soluble polymers with different affinities for metals, are often used as stabilizers in the preparation of metal nanoparticles. Different stabilizers and reducing agents were used to control not only the reduction rate of metal ions but also the aggregation process of metal atoms, so that the size and shape of metal nanoparticles could be manipulated. The reduction of $PtCl_6^{2-}$ with aqueous methanol (see eq 2) in the presence of poly(*N*-vinyl-2-pyrrolidone) (PVP) yielded well-dispersed Pt nanoparticles. The average size of Pt_n was measured to be about 3.4 nm from Figure 1a. The Pt nanoparticles were almost uniform.

$$H_2Pt_2Cl_6 + 2CH_3OH \rightarrow Pt^0 + 2HCHO + 6HCl \quad (2)$$

As stated in the Experimental Section, H_2 and Nafion were used as reducing reagent (see eq 3) and stabilizer, respectively, to prepare Pt_n^{ag}. In comparison with PVP, Nafion may not adhere

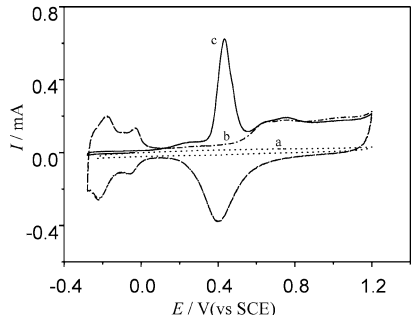

Figure 2. Cyclic voltammograms of bare GC (a), Pt_n^{ag}/GC (b), and the oxidation of adsorbed CO on Pt_n^{ag}/GC (c) in 0.1 M H_2SO_4, sweep rate 50 mV s^{-1}.

on Pt nanoparticles as strong as PVP does. Figure 1b illustrated that the synthesized material is in fact an agglomerate of Pt nanoparticles.

$$H_2Pt_2Cl_6 + 2H_2 \rightarrow Pt^0 + 6HCl \qquad (3)$$

The mean size of the aggregates of Pt nanoparticles is measured to be about 400 nm.

2. Cyclic Voltammetric Studies of CO Adsorbed on a Pt_n^{ag}/GC Electrode. Figure 2 shows the stable cyclic voltammograms (CV) of (a) bare GC and (b) Pt_n^{ag}/GC, as well as (c) the oxidation of CO adsorbed on Pt_n^{ag}/GC in 0.1 M H_2SO_4. Well-known CV features of a Pt polycrystalline electrode can be observed from Figure 2b. Two distinct pairs of current peak around −0.02 and −0.16V are the characteristic potentials for hydrogen adsorption−desorption. Pt oxide is formed in the positive-going potential scan up to potentials above 0.6V. In the reverse scan, a reduction current peak of Pt oxide is recorded at 0.4 V. It can be seen from Figure 2C that the hydrogen adsorption−desorption current is suppressed when the electrode surface was covered with CO. The onset potential of CO oxidation is seen at about 0.11 V, and the oxidation occurs in a small current peak lying between 0.1 and 0.33 V, following a large current peak centered around 0.47 V. It is worth noting that the onset potential of CO oxidation a bulk polycrystalline Pt is 0.51 V and the current peak locates around 0.55 V under the same conditions. The results demonstrated that the agglomerates of Pt nanoparticles exhibit good electrocatalytic properties. It may be pointed out that the CV of a Pt_n/GC electrode, and those of CO_{ad} oxidation on the Pt_n/GC exhibit similar characteristic to those of Pt_n^{ag}/GC.

3. In Situ FTIRS Studies. Figure 3 shows MS-FTIR spectra for CO adsorbed on a bulk Pt electrode in 0.1 M H_2SO_4 solution; two IR bands were recorded. The negative-going band around 2070 cm^{-1} is assigned to IR absorption of linearly bonded CO (CO_L) at E_S varied from −0.25 to 0.2 V. The center of this band shifts to higher wavenumbers with the increase of E_S wherein two series of data are linearly correlated to give a slope $d\nu_{CO}/dE$ = 29.4 cm^{-1} V^{-1}, as shown in Figure 6a, which represents the electrochemical Stark shift rate. This rate is nearly the same as that reported in the literature.[35−37] Except for the CO_L band, a positive-going band near 2345 cm^{-1} in Figure 3 is ascribed to the IR absorption of CO_2 species at E_R (0.7V). The results indicate that CO_{ad} has been oxidized at E_R to afford CO_2 determined by the 2345 cm^{-1} band at E_R. This conclusion is valid because no CO_2 and CO species presented initially at E_S in the thin layer solution between the electrode and IR window. It has been confirmed that, through a series of spectra recorded consecutively at E_R, most CO_2 species produced from CO_{ad} oxidation can be retained in the thin layer between the electrode and IR window due to a big resistance of diffusion. As a consequence, the integrated intensity of the CO_2 band (A_{CO_2}) can be taken as a measure of the quantity of CO_{ad}. The normalized intensity of the CO_{ad} band ($NA_{CO_{ad}}$) can be thus defined as $A_{CO_{ad}}/A_{CO_2}$, i.e., $(NA_{CO_{ad}})_{Pt} = (A_{CO_{ad}}/A_{CO_2})_{Pt}$. It is necessary to note that for CO adsorbed on a bulk Pt electrode, the CO_L band at ∼2070 cm^{-1} always appears in the opposite direction to the CO_2 band at 2345 cm^{-1} under the present experimental conditions. This is also in accordance with the predication of eq 1.

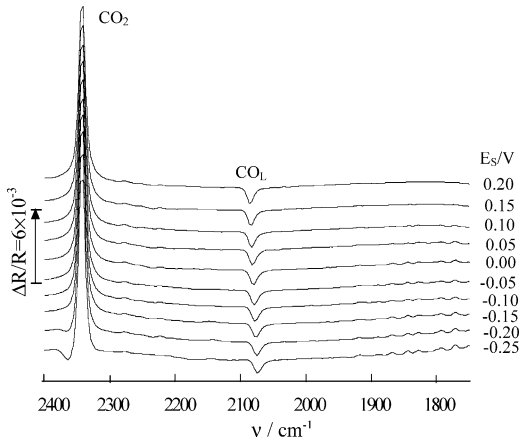

Figure 3. In situ FTIR spectra of CO adsorbed on a bulk Pt electrode in 0.1 M H_2SO_4, E_R = 0.9 V. E_S is indicated for each spectrum.

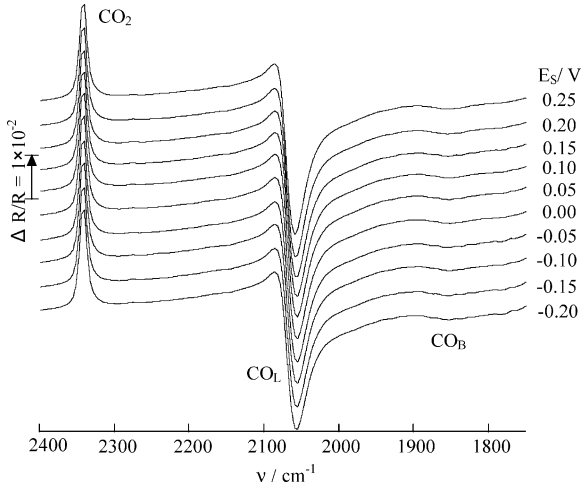

Figure 4. In situ FTIR spectra of CO adsorbed on the Pt_n/GC electrode in 0.1 M H_2SO_4, E_R = 0.9 V. E_S is indicated for each spectrum.

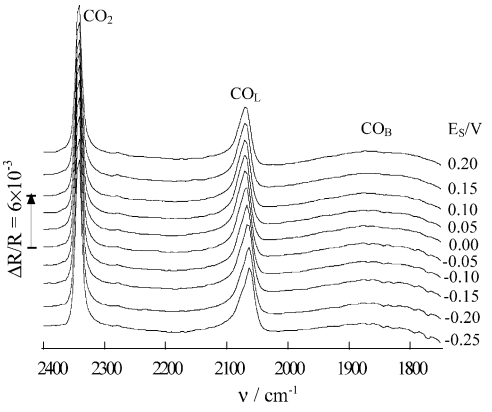

Figure 5. In situ FTIR spectra of CO adsorbed on the Pt_n^{ag}/GC electrode in 0.1 M H_2SO_4, E_R = 0.6 V. E_S is indicated for each spectrum.

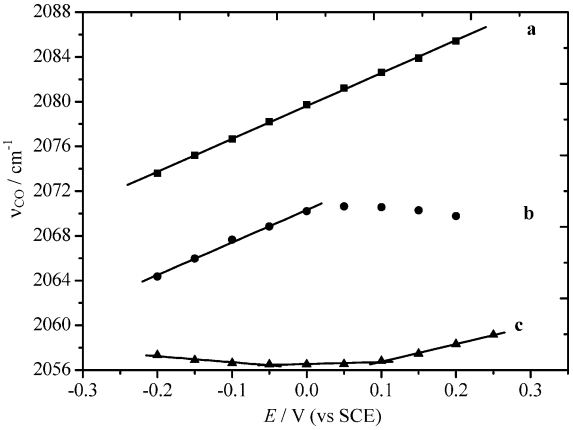

Figure 6. Plots of ν_{CO} versus E for CO adsorbed on (a) a bulk Pt electrode, (b) a Pt_n^{ag}/GC electrode, and (c) Pt_n/GC electrodes.

In the case of CO adsorbed on a Pt_n/GC electrode, the MS−FTIR spectra display three IR bands (Figure 4), i.e., the positive-going CO_2 band (around 2345 cm^{-1}), the negative-going CO_L band (around 2059 cm^{-1}), and a small but broad negative-going band near 1855 cm^{-1} that is assigned to IR absorption of bridge bonded CO (CO_B). It can be seen that the IR bands of CO_{ad} (CO_L and CO_B) and CO_2 in Figure 4 appear in the directions analogous with those in Figure 3. However, the IR band of CO_L on the Pt_n/GC electrode is not only slightly red-shifted (from 2070 to 2059 cm^{-1}), but also significantly enhanced. The appearance of CO_B in spectra is certainly due to this enhanced IR absorption of CO adsorbed on Pt_n/GC. To evaluate quantitatively the effect of IR enhancement absorption on Pt nanoparticles, we define an enhancement factor (Δ_{IR}) that is equal to the ratio of the normalized CO_{ad} intensity on the Pt_n/GC electrode versus that on a bulk Pt surface, i.e.,

$$\Delta_{IR} = \frac{(NA_{COad})_{Pt_n/GC}}{(NA_{COL})_{Pt}} = \frac{A_{Pt_n}^{CO_{ad}}/GC}{A_{Pt_n}^{CO_2}/GC} \frac{A_{Pt}^{CO_2}}{A_{Pt}^{CO_L}} \qquad (4)$$

where $A_{Pt_n/GC}^{CO_{ad}}$ and $A_{Pt_n/GC}^{CO_2}$ refer to integrated intensities of the CO_{ad} ($CO_L + CO_B$) and CO_2 bands, respectively, measured in IR spectra of Pt_n/GC electrode; $A_{Pt}^{CO_L}$ and $A_{Pt}^{CO_2}$ are the integrated intensities of the CO_L and CO_2 bands, respectively, acquired in the IR spectra of a bulk Pt electrode. From eq 4, the calculated $\Delta_{IR} = 31$ indicates that the IR absorption of CO_{ad} has been enhanced 31 times on Pt nanoparticle electrode. Besides the enhancement of IR absorption of CO_{ad}, the CO_{ad} bands are broadened on Pt_n/GC. The value of the full width at half-maximum (FWHM) of the CO_L band in Figure 4 is measured to be 40 cm^{-1}, which is 25 cm^{-1} larger than that measured from the spectrum of bulk Pt (15 cm^{-1}), implying an increasing discreteness of vibration energy states in the CO−Pt_n/GC system. Moreover, the C−O stretching frequency of CO_L is shifted irregularly when E_S is increased. We can see that the variation of the CO_L band center versus E_S exhibits a concave curve (see Figure 6c) in contrast to the linear variation observed for CO adsorbed on bulk Pt electrode (see Figure 6a). Similar nonmonotonic behavior has been reported in cases of a low CO coverage adsorbed on Pt single-crystal electrodes.[38−41] For CO adsorbed on Pt(100), an essential linear $\nu_{CO_L}-E$ plot is obtained at potentials prior to the onset of electrooxidation of CO in the saturation layer. Markedly different behavior, however, is obtained at lower coverages. A surprising nonmonotonic $\nu_{CO_L}-E$ correlation has been observed: the slope of this correlation is negative over the potential range of hydrogen adsorption, but it changes to positive from the onset of hydrogen desorption.[38] Similarly, the potential dependent response of ν_{CO_L} at low CO coverages adsorbed on Pt (335) is nonlinear.[39−41] The nonlinear $\nu_{CO_L}-E$ plot is attributed to the effect of competitive hydrogen coadsorption in the low potentials range.[38,41] As described in the Experimental Section, an extra Nafion film was applied over Pt nanoparticles in the preparation of the Pt_n/GC electrode. This may lead to a below-the-saturation level of CO adsorbed on Pt_n/GC electrode and also to a competitive adsorption between hydrogen and CO at low potentials. As a consequence it results in the nonmonotonic $\nu_{CO}-E$ behavior. Interestingly, such $\nu_{CO}-E$ behaviors have also been reported for carbon-supported platinum nanoparticles with low-coverage CO.[42] These results demonstrate that CO adsorbed on dispersed Pt nanoparticles yields enhanced infrared absorption (EIRA). In this case, the direction of the CO_{ad} bands is the same as that of the CO_L band on bulk Pt.

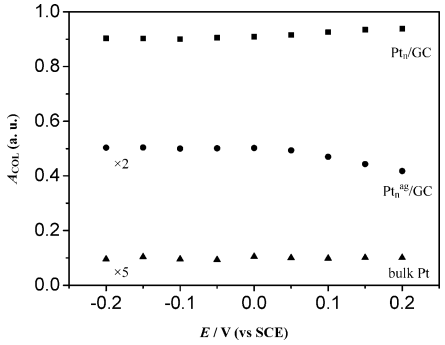

Figure 7. Plots of integrated band intensity of linearly adsorbed CO on bulk Pt, Pt_n^{ag}/GC, and Pt_n/GC electrodes.

A series of IR spectra of CO adsorbed on Pt_n^{ag}/GC in 0.5 M H_2SO_4 as the function of potential show dramatic changes in spectral features; see Figure 5. The IR features differ from those of CO adsorbed on bulk Pt on the following respects. First, the CO_{ad} bands become positive-going; i.e., the direction of the CO_L and CO_B bands is inverted to the direction of antiabsorption, and consequently shows the same direction as that of the CO_2 bands. Second, the intensity of the CO band is increased significantly, giving an enhancement factor of $\Delta_{IR} = 9$ according to eq 4. Third, the FWHM of the CO_L band is increased to 25 cm^{-1} from the value of 15 cm^{-1} of that measured on a bulk Pt. These are typical IR features of abnormal infrared effects (AIREs) that are observed initially for CO adsorbed on electrodes of nanostructured thin films of platinum metals and alloys.[22−25] Figure 6b shows the plot of ν_{CO_L} with E for CO adsorbed on Pt_n^{ag}/GC. The electrochemical Stark shift rate is calculated to be 26.1 cm^{-1} V^{-1} from the linear part of the correlation up to $E = 0.0$ V; above this E value, the variation of ν_{CO_L} abruptly deviated from the linear relationship and decreased slightly. This is obviously due to a partial oxidation of CO adsorbed on the agglomerates of Pt nanoparticle, as also can be elucidated in CV curves (Figure 2). The variations of the integrated CO_L band intensity with E on bulk Pt, Pt_n^{ag}/GC, and Pt_n/GC electrodes are shown in Figure 7. We can see that the A_{CO_L} on Pt_n^{ag}/GC began to decrease when the electrode potential was increased above 0.0 V, confirming the partial oxidation of CO_{ad} on this electrode. However, the integrated band intensity of CO_L species adsorbed on bulk Pt and Pt_n/GC remains almost unchanged in the whole potential range from −0.2 to +0.2 V. It is worth mentioning that we have revealed also that the agglomerates of Pt nanoparticles exhibited significant electrocatalytic activity in methanol oxidation.[43] It is interesting to see (Figure 6) that the vibration frequency of CO_L

(ν_{CO_L}) is red-shifted from bulk Pt to agglomerates of Pt nanoparticles, and then to dispersed Pt nanoparticles, illustrating clearly the effect of agglomeration of Pt nanoparticles.

The above results revealed that the dispersed Pt nanoparticles and the agglomerate of Pt nanoparticles exhibit significantly different IR optical properties. The former gives rise to an enhanced IR absorption, but the latter yields abnormal infrared effects. In the agglomerate of Pt nanoparticles, strong interaction between Pt nanoparticles may exist, which may increase the confinement of the movement of electrons and lead to possible resonance effects. On another side, CO adsorbed on the agglomerate may present uniquely collective interactions between CO and Pt nanoparticles inside the agglomerate. It is evident that the enhancement of IR absorption of CO adsorbed on both Pt_n/GC and Pt_n^{ag}/GC electrodes can be attributed to the effect of the nanometer size of the material and that the antiabsorption in the AIREs observed exclusively on the Pt_n^{ag}/GC electrode may be ascribed primarily to the strong interaction between Pt nanoparticles and the collective interaction between CO adsorbate and Pt nanoparticles inside the agglomerates.

Conclusions

We have prepared Pt nanoparticles (Pt_n) and their agglomerates (Pt_n^{ag}) through reduction of $H_2Pt_2Cl_6$ under different conditions. The electrodes were prepared by applying a prescribed quantity of Pt_n and Pt_n^{ag}, respectively, on the surface of the GC substrate. Using CO adsorption as the molecular-probe reaction, both electrocatylic and IR optical properties of the prepared nanomaterials were investigated using cyclic voltammetry and in situ FTIR reflection spectroscopy. Cyclic voltammetric results demonstrated that electrodes of Pt nanoparticles (Pt_n) and their agglomerates (Pt_n^{ag}) both possess high activity for electrooxidation of adsorbed CO species. The voltammograms show that the current peak potential of CO_{ad} oxidation on the Pt_n^{ag}/GC electrode is shifted negatively by 80 mV in comparison with the value measured on a bulk Pt electrode. In situ FTIRS studies illustrated that the Pt nanoparticles and the agglomerate exhibit different IR properties for CO_{ad} adsorption. In comparison to CO adsorbed on a bulk Pt electrode, a phenomenon of enhanced IR absorption (EIRA) was observed for CO on Pt_n/GC, in which its absorption intensity is enhanced 31 times and the FWHM of the CO_L band is increased to 40 cm^{-1}, which is 25 cm^{-1} larger than the FWHM of CO_L band measured on a bulk Pt. However, abnormal IR effects (AIREs) was discovered in the study of CO on Pt_n^{ag}/GC; namely, except for the enhancement IR absorption and the increase in FWHM of CO_{ad} bands, the direction of CO_{ad} bands was inverted to the direction of antiabsorption in comparison with that of CO adsorbed on dispersed Pt nanoparticles. The different IR properties between the Pt nanoparticles and its agglomerate suggest that the EIRA phenomenon is mainly related to the effect of the nanometer size of the material and that the antiadsorption in the AIREs may be caused by the strong interaction between Pt nanoparticles and the collective interaction between CO adsorbate and Pt nanoparticles inside the agglomerate. This study has thrown a light on revealing the origin of the abnormal infrared effects, and on understanding the nanometer size effect of agglomeration of Pt nanoparticles as well.

Acknowledgment. The present study was supported by grants from the National Natural Science Foundation of China (20021002, 90206039), the State Education Ministry of China (01101), and by the National key basic research and development program (2002CB211804).

References and Notes

(1) Ahmadi, T. S.; Wang, Z. L.; Green, T. C.; Henglein, A. M.; El-Sayed, A. *Science* **1996**, *272*, 1924.
(2) Collier, C. P.; Saykally, R. J.; Shiang, J. J.; Henrichs, S. E.; Heath, J. R. *Science* **1997**, *277*, 1978.
(3) Emory, R. S.; Haskins, W. E.; Nie, S. *J. Am. Chem. Soc.* **1998**, *120*, 8009.
(4) Kim, Y.; Johnson, R. C.; Hupp, J. T. *Nano. Lett.* **2001**, *1*, 167.
(5) Novak, J. P.; Nickerson, C.; Franzen, S.; Feldheim, D. L. *Anal. Chem.* **2001**, *73*, 5758.
(6) Toshima, N.; Yonezawa, T. *New J. Chem.* **1998**, *22*, 1179.
(7) Johnson, B. F. G.; McIndoe, J. S. *Coord. Chem. Rev.* **2000**, *200*−*202*, 901.
(8) Roucoux, A.; Schulz, J.; Patin, H. *Chem. Rev.* **2002**, *102*, 3757
(9) Hirai, H. *J. Macromol. Sci.-Chem.* **1979**, *A13* (5), 633.
(10) Chen, C.-W.; Akashi, M. *Langmuir* **1997**, *13*, 6465.
(11) Teranishi, T.; Hosoe, M.; Tanaka, T.; Miyake, M. *J. Phys. Chem. B* **1999**, *103*, 3818.
(12) Bonet, F.; Delmas, V.; Grugeon, S.; Herrera Urbina, R.; Silvert, P.-Y. *Nanostruct. Mater.* **1999**, *11*, 1277.
(13) Tu, W. X.; Liu, H. F. *J. Mater. Chem.* **2000**, *10*, 2207.
(14) Chen, C.-W.; Takezako, T.; Yamamoto, K.; Serizawa, T.; Akashi, M. *Colloids Surf. A: Physicochem. Eng. Aspects* **2000**, 169, 107.
(15) Mandal, S.; Selvakannan, PR.; Roy, D.; Chaudhari, R. V.; Sastry, M. *Chem. Commun.* **2002**, 3002.
(16) Storhoff, J. J.; Elghanian, R.; Mucic, R. C.; Mirkin, C. A.; Letsinger, R. L. *J. Am. Chem. Soc.* **1998**, *120*, 1959.
(17) Lazarides, A. A.; Schatz, G. C. *J. Phys. Chem. B* **2000**, *104*, 460.
(18) Shipway, A. N.; Lahav, M.; Gabai, R.; Willner, I. *Langmuir* **2000**, *16*, 8789.
(19) Kamat, P. V. *J. Phys. Chem. B* **2002**, *106*, 7729.
(20) Norman, T. J.; Grant, C. D.; Magana, D.; Zhang, J. Z.; Liu, J.; Cao, D. L.; Bridges, F.; Buuren, A. V. *J. Phys. Chem. B* **2002**, *106*, 7005.
(21) Mcnicol, B. D.; Rand, D. A. J.; Williams, K. P. *J. Power Sources* **1999**, *83*, 15.
(22) Lu, G. Q.; Sun, S. G.; Chen, S. P.; Li, N. H.; Yang, Y. Y.; Tian, Z. W. In *Electrode Processes IV*; Wieckowski, A., Itaya, K., Eds.; The Electrochemical Society, Inc.: Pennington, NJ, 1996; pp 96−8, 436.
(23) Lu, G. Q.; Sun, S. G.; Chen, S. P.; Cai, L. R. *J. Electroanal. Chem.* **1997**, *421*, 19.
(24) Lu, G. Q.; Sun, S. G.; Cai, L. R.; Chen, S. P.; Tian, Z. W.; Shiu, K. K. *Langmuir* **2000**, *16*, 778.
(25) Lu, G. Q.; Cai, L. R.; Sun, S. G.; He, J. X. *Chin. Sci. Bull.* **1999**, *44*, 1470.
(26) Zheng, M. S.; Sun, S. G. *J. Electroanal. Chem.* **2001**, *500*, 223.
(27) Zheng, M. S.; Sun, S. G.; Chen, S. P. *J. Appl. Electrochem.* **2001**, *31*, 749.
(28) Chen, Z.; Sun, S. G.; Zhou, Z. Y.; Ding, N. *Chin. Sci. Bull.* **2001**, *46*, 1439.
(29) Lin, W.-G.; Sun, S.-G.; Zhou, Z.-Y.; Chen, S.-P.; Wang, H.-C. *J. Phys. Chem. B* **2002**, *106*, 11778.
(30) Hartstein, A.; Kirtly, J. R.; Tsang, J. C.*Phys. Rev. Lett.* **1980**, *45*, 201.
(31) Osawa, M.; Ikeda, M. *J. Phys. Chem.* **1991**, 95, 9914.
(32) Sun, S.-G.; Cai, W.-B.; Wan, L.-J.; Osawa, M. *J. Phys. Chem. B* **1999**, *103*, 2460.
(33) Jiang, Y.-X.; Sun, S.-G.; Ding, N. *Chem. Phys. Lett.* **2001**, *344*, 463.
(34) Lin, W. F.; Sun, S. G. *Electrochim. Acta* **1996**, *41*, 803.
(35) Bewick, A. *J. Electroanal. Chem.***1983**, *150*, 481.
(36) Kunimatsu, K.; Seki, H.; Golden, W. G.; Gordon, J. G., II; Philpott, M. R. *Surf. Sci.* **1985**, *158*, 596.
(37) Love, J. G.; Mcquillan, A. J. *J. Electroanal. Chem.* **1989**, *274*, 263.
(38) Chang, S. C.; Weaver, M. J. *J. Phys. Chem.* **1990**, *94*, 5095.
(39) Kim, C. S.; Korzeniewski, C. *Anal. Chem.* **1997**, *69*, 2349.
(40) Kim, C. S.; Korzeniewski, C.; Tornquist, W. J. *J. Chem. Phys.* **1994**, *100*, 628.
(41) Kim, C. S.; Tornquist, W. J.; Korzeniewski, C. *J. Phys. Chem. B* **1993**, *97*, 6484.
(42) Park, S.; Wasileski, S. A.; Weaver, M. J. *J. Phys. Chem. B* **2001**, *105*, 9719.
(43) Chen, W.; Sun, S.-G.; Si, D.; Chen, S.-P. *Acta Phys.-Chim. Sin.* **2003**, *19*, 441.